# Secondary ion formation on indium under nuclear and electronic sputtering conditions

Matthias Herder, Philipp Ernst, Lars Breuer, Markus Bender, Daniel Severin, and Andreas Wucher

Citation: Journal of Vacuum Science & Technology B **36**, 03F110 (2018); doi: 10.1116/1.5018721
View online: https://doi.org/10.1116/1.5018721
View Table of Contents: http://avs.scitation.org/toc/jvb/36/3
Published by the American Vacuum Society

**Articles you may be interested in**

Polymer-matrix nanocomposites bombarded by large Ar clusters and low energy Cs ions: Sputtering and topography development
Journal of Vacuum Science & Technology B, Nanotechnology and Microelectronics: Materials, Processing, Measurement, and Phenomena **36**, 03F118 (2018); 10.1116/1.5015989

Relationships between crater and sputtered material characteristics in large gas cluster sputtering of polymers: Results from molecular dynamics simulations
Journal of Vacuum Science & Technology B, Nanotechnology and Microelectronics: Materials, Processing, Measurement, and Phenomena **36**, 03F109 (2018); 10.1116/1.5012981

ToF-SIMS analysis of ion implanted standard to quantify insecticide in mosquito netting with cesium and argon gas cluster sputtering beams
Journal of Vacuum Science & Technology B, Nanotechnology and Microelectronics: Materials, Processing, Measurement, and Phenomena **36**, 03F111 (2018); 10.1116/1.5011751

Effect of kinetic energy and impact angle on carbon ejection from a free-standing graphene bombarded by kilo-electron-volt $C_{60}$
Journal of Vacuum Science & Technology B, Nanotechnology and Microelectronics: Materials, Processing, Measurement, and Phenomena **36**, 03F112 (2018); 10.1116/1.5019732

Principal component analysis image fusion of TOF-SIMS and microscopic images and low intensity secondary ion enhancement by pixel reduction
Journal of Vacuum Science & Technology B, Nanotechnology and Microelectronics: Materials, Processing, Measurement, and Phenomena **36**, 03F113 (2018); 10.1116/1.5013218

Latest improvements in isotopic uranium particle analysis by large geometry–secondary ion mass spectrometry for nuclear safeguards purposes
Journal of Vacuum Science & Technology B, Nanotechnology and Microelectronics: Materials, Processing, Measurement, and Phenomena **36**, 03F108 (2018); 10.1116/1.5016943

# Secondary ion formation on indium under nuclear and electronic sputtering conditions

Matthias Herder,[a] Philipp Ernst, and Lars Breuer
*Fakultät für Physik, Universität Duisburg-Essen, 47048 Duisburg, Germany*

Markus Bender and Daniel Severin
*GSI Helmholtz Zentrum für Schwerionenforschung, 64291 Darmstadt, Germany*

Andreas Wucher
*Fakultät für Physik, Universität Duisburg-Essen, 47048 Duisburg, Germany*

(Received 8 December 2017; accepted 26 January 2018; published 13 February 2018)

The electronic sputtering of indium under swift heavy ion bombardment is investigated using time of flight secondary ion mass spectrometry in combination with 157 nm laser postionization. Secondary ion and neutral mass spectra generated under the impact of 4.8 MeV/u $^{48}Ca^{10+}$ ions are analyzed in order to determine the ionization probability of the emitted indium atoms, and the results are compared to those measured under nuclear sputtering conditions via bombardment by 5 keV $Ar^{+}$ primary ions. The influence of surface contamination on the ionization probability is studied by comparing (1) a pristine surface covered by a native oxide layer, (2) a kilo-electron-volt sputter-cleaned surface, and (3) a controlled oxygen coverage established by dosing the precleaned surface with $O_2$. It is found that the native oxide layer increases the ionization probability for both kilo-electron-volt and mega-electron-volt primary ions. In contrast, oxygen deposited on a sputter-cleaned surface results in the well-known matrix effect for kilo-electron-volt ions, but has no influence on the ionization probability for the mega-electron-volt ions. In the case of a thoroughly sputter-cleaned surface a four- to sevenfold higher ionization probability for indium atoms is found for 4.8 MeV/u $^{48}Ca^{10+}$ as compared to 5 keV $Ar^{+}$ bombardment. *Published by the AVS.* https://doi.org/10.1116/1.5018721

## I. INTRODUCTION

When an ion impinges on a solid, it can transfer energy to the solid via collision with the atoms ("nuclear stopping") or excitation of the electrons ("electronic stopping"). This can enable constituents of the solid to overcome their binding energy and propagate away from the surface. This process is called "sputtering." Two different sputtering regimes are distinguished, depending on which the energy loss channel is prevalent. At low (keV) kinetic energies, the primary ion interacts with the solid primarily by (elastic) collisions, which initiates a collisional cascade. Recoils of this cascade can lead to the emission of secondary particles at the surface. In the following, this process is termed "collisional sputtering." Part of the sputtered material is emitted in a charged state, and the resulting secondary ions are utilized in secondary ion mass spectrometry (SIMS) as an established surface analysis technique. In the high kinetic energy limit, collisions with the target nuclei become improbable. Consequently, the ion moves through the solid along a straight line while depositing energy mainly into the electronic subsystem. "Electronic sputtering" can occur, if a sufficient amount of this energy in transferred to the lattice, for example, by electron-phonon coupling.

Currently, direct observation of the dynamics of the sputtering process at the atomic scale is only possible in the model calculations. Experiments are limited to investigating the asymptotic state in the form of the ion-induced damage to the sample and secondary particles that are emitted. Quantities like the amount and composition, as well as the angular and velocity distribution of the sputtered material, can be obtained and compared to the predictions of model calculations. Extensive research has been conducted for both regimes.[1] As a result, the collisional sputtering is now fairly well understood.[2,3] In the electronic sputtering regime, the sputter yield, i.e., the average number of target atoms removed from the surface per single ion impact, and the angular distribution of the sputtered material have been studied for a variety of projectile-target combinations using the catcher-foil technique.[4–15] An open question, however, regards the characterization of the sputtered material flux both in terms of composition (atoms, molecules, clusters,…) and charge state (secondary ions and neutral particles, respectively). For secondary ions, mass spectra, as well as the velocity magnitude and direction of the emitted particles have be measured with time-of-flight (ToF) mass spectrometry methods,[16–31] but the distribution of the corresponding neutral clusters is still unknown.[18,21,30] Consequently, improving the understanding of the ion formation process under electronic sputtering conditions would be beneficial for connecting findings on secondary ions with the total sputtered flux. In this context, it is useful to introduce the ionization probability as the probability for a specific secondary atom, cluster or molecule to be emitted in a charged state. The ionization probability can be specified for positively and negatively charged ions separately and may depend on the angle and velocity of the emitted particle. Another important factor is the dependence on the chemical environment the particle was emitted from, which has been

[a]Electronic mail: matthias.herder@uni-due.de

termed "matrix effect." To quantify the ionization probability, it is necessary to detect the secondary ions and neutrals under identical experimental conditions in a mass-resolved manner. For that purpose, the neutral particles must be postionized after their emission from the surface in order to render them accessible for mass spectrometric detection, a technique which is generally referred to as secondary neutral mass spectrometry (SNMS). Among various possible postionization methods,[32–40] we have frequently applied single-photon ionization in combination with a ToF mass spectrometer to investigate ionization probabilities of sputtered particles.[37,41–50] For atoms and clusters emitted from a clean metal surface under kilo-electron-volt ion irradiation, the ionization probability is generally found to be small ($<10^{-3}$) for atoms and to increase with increasing cluster size.[37] It is well known that particularly the atomic ionization probabilities can be strongly influenced by surface contamination. A strong example of this influence is the so-called oxygen matrix effect, where the oxidation of a metallic or semiconductor surface leads to an increase of the positive ionization probability observed in kilo-electron-volt SIMS experiments by several orders of magnitude.[51–53] So far, it is unclear whether this enhancement also works under electronic sputtering conditions. In this work, we therefore investigate the ionization probability of indium atoms emitted from a polycrystalline indium surface under electronic sputtering conditions with a particular emphasis on the influence of surface contamination. For that purpose, a pristine surface is first sputter-cleaned by kilo-electron-volt argon ion bombardment in order to remove the native oxide layer. Then, the oxygen surface coverage is varied in a systematic manner by dosing the surface with $O_2$, and its influence on the ionization probability is measured. The results are interpreted in terms of the particle emission mechanism under electronic sputtering.

## II. EXPERIMENT

The experimental setup[54] used in these experiments is located at the M1 beam line of the Universal Linear Accelerator (UNILAC) at the Helmholtz Centre for Heavy Ion Research (GSI) in Darmstadt, Germany. For this experiment, we used a pulsed 4.8 MeV/u $^{48}Ca^{10+}$ beam with a pulse length of 5 ms and a repetition rate of 2.5 Hz. The UNILAC beam was focused to a spot of 7 mm diameter using a fluorescent target. The UNILAC beam current averaged over time was measured to be about $3 \times 10^{-9}$ A using a Faraday cup. From these parameters, we deduce a pulse particle current of 24 nA equivalents, a pulse particle flux of $3.9 \times 10^{11}$ ions/cm$^2$ s, and a fluence of $2 \times 10^9$ ions/cm$^2$ per pulse. In addition to the swift heavy ion (SHI) beam line, the setup is equipped with a 5 keV $Ar^+$ ion source. Both ion beams impinge with the same polar angle of 45° onto the surface but with a different azimuth angle with respect to the surface normal. The $Ar^+$ current was measured with a Keithley source meter using a bias voltage of +100 V to suppress secondary electron emission. The $Ar^+$ beam was defocused and its size measured with a fluorescent target. The $Ar^+$ current of 64 nA and the 3 mm beam diameter yield a ion flux density of $5.7 \times 10^{12}$ ion/cm$^2$ s.

The experiment was conducted using a home-built reflectron ToF mass spectrometer described in detail elsewhere.[55] The spectrometer is mounted with its optical axis orthogonal to the sample surface. The secondary ions are extracted by pulsing the sample potential to 1600 V using a fast high voltage switch (Behlke HTS 31 GSM) with a rise time of about 20 ns. The reflection of the ions inside the ToF spectrometer allows for ions starting at various distances above the surface to be focused into a sharp time peak with a mass resolution ($m/\Delta m$) of about 300. The reflection voltage of 1450 V was set 150 V below the extraction voltage to ensure that only ions starting from a minimal distance of 1 mm above the sample can reach the detector. The detector is a multichannel plate (MCP) Chevron stack with the front set at a 4000 V postacceleration voltage to increase the detection efficiency. The active area of 20 mm diameter in combination with an Einzel lens at the ToF entrance limits the starting location to a 1 mm diameter cylinder. Due to the time refocusing properties of the reflectron, ions starting from more than about 2 mm above the sample surface are dispersed in time and do not contribute to the sharp flight time peaks. To summarize, this means that only ions starting in a cylindrical volume of 1 mm diameter and 1 mm height located at about 1 mm above the surface can contribute to the measured signal. In the following, this will be referred to as the sensitive volume. The MCP output signal was recorded with a fast transient digitizer board (Signatec PX1500) in 1 ns steps. The input range of 500 mV is digitized in discrete values from 0 to 255, which in the following will be called "cts." One ct therefore describes a 2 mV voltage step at the 50 Ω input resistor of the digitizer, which should not be confused with the detection of a single ion. To enhance the signal statistics, multiple mass spectra are summarized and later divided by the number of repetitions, which results in the unit "cts/rep" used for the display of the measured signal.

To detect the secondary neutral particles, a vacuum ultraviolet laser pulse is fired into the sensitive volume with the laser beam directed parallel to the sample surface. The employed $F_2$ excimer laser was operated at a wavelength of 157 nm corresponding to a photon energy of 7.9 eV, which is sufficient for a single photon ionization of indium atoms and clusters. The laser has a pulse length of 4–7 ns and energy of 1.1 mJ, which was monitored with an internal energy monitor and a photo-detector located behind the sample in the ultrahigh vacuum (UHV) chamber. A $CaF_2$-lens with a focal length of 250 mm was used to focus the laser beam to a spot of about 1 mm diameter. If the laser is fired at the exact time the ion extraction field is switched on, the ToF-spectrometer cannot distinguish between secondary ions and postionized neutrals. However, in this experiment, the laser was fired 115 ns after the extraction field in order to separate the signals of secondary ions and postionized neutrals in the flight time spectrum. In addition, mass spectra were always recorded both with (SNMS) and without (SIMS) firing the laser, so the signals of the postionized neutrals can be identified and extracted by subtracting the SIMS signals in the SNMS spectra.

Six different types of mass spectra are acquired for each measurement, namely, two under 4.8 MeV/u $^{48}Ca^{10+}$ ion bombardment (mega-electron-volt-SIMS and -SNMS), two under 5 keV $Ar^+$ ion bombardment (kilo-electron-volt-SIMS and SNMS), and two without any primary ion bombardment (background). The background spectrum taken with the laser being fired represents the spectrum generated by ionization of the residual gas in the UHV chamber, which, for instance, can be used to monitor the sample temperature during SHI irradiation since heating of the sample will result in desorption of molecules and thus a rise of the residual gas pressure. All six mass spectra are generated in an interleaved manner, taking into account the different repetition rate limits of the UNILAC (50 Hz maximum, 2.5 Hz in this experiment), the laser (500 Hz) and the ToF instrument (10 kHz). To sputter clean the surface during measurements, the 5 keV $Ar^+$ ion source can be switched on between the data acquisition cycles, a technique that will be referred to as "interleaved sputter cleaning" in the following.

The sample was a polycrystalline indium foil clamped to the sample holder by means of a molybdenum mask with a 2 mm diameter aperture to ensure that the signal originates from an area that is homogeneously exposed to both ion beams. The signals of the pristine surface were recorded for both primary ion species following the transfer of the sample into the UHV chamber. The contaminations from the exposure to ambient air and the native oxide on the surface were then removed using the interleaved sputter cleaning method while continuously monitoring all signals. As the next step, the surface was exposed to oxygen by flooding the UHV chamber with $O_2$ gas to a partial pressure of $5 \times 10^{-7}$ mbar using a leak valve. The partial pressure and purity of the $O_2$ gas was monitored with a quadrupole mass spectrometer. The residual gas pressure in the UHV chamber was in the order of $10^{-10}$ mbar and there was no increase detected for other signals during the $O_2$ gas inlet. During the oxygen exposition, signals for both ion species were again continuously recorded, albeit in this case with the interleaved sputter cleaning turned off. After reaching a plateau for the oxygen related SIMS and SNMS signals, the $O_2$ gas inlet was stopped and the surface was sputter-cleaned with 5 keV $Ar^+$ for 11.5 h without a continuous recording of signals to limit the fluence for the $^{48}Ca^{10+}$ ions. Finally, signals for the thoroughly (11.5 h) sputter-cleaned surface were recorded to recheck the previous measurement.

## III. RESULTS AND DISCUSSION

As outlined in Sec. I, the goal of this paper is to determine the influence of surface chemistry on the ionization probability of atoms sputtered under swift heavy ion bombardment and compare the results to those observed under kilo-electron-volt rare gas ion impact. This section is therefore organized as follows: First, we discuss the mass spectra measured for secondary ions (SIMS) and postionized neutrals (SNMS) under the various surface conditions employed in this work (pristine surface as introduced into the vacuum, sputter-cleaned surface and reoxidized surface) in order to identify the relevant secondary ion (superscript "+" or "−") and postionized neutral (superscript "0") signals to follow in the remainder of the discussion. In Subsection III B, we then discuss sputter depth profiles showing the variation of relevant signals reflecting the removal of initial surface contamination and the native oxide layer in the course of the sputter cleaning process. Subsection III C is then devoted to the reoxidation experiment, where the sputter-cleaned surface is oxidized in a controlled manner by oxygen adsorption.

### A. Mass spectra

SNMS spectra recorded for the pristine, sputter-cleaned and oxidized indium surface are shown in Fig. 1 for 5 keV $Ar^+$ (a)–(c) and 4.8 MeV/u $^{48}Ca^{10+}$ (d)–(f) bombardment. The corresponding background spectra are omitted, because no significant residual gas signals were present. Keep in mind that the SNMS spectrum also contains the secondary ion signals, which appear separated from the postionization peaks by a 115 ns time delay (corresponding to about 1 amu apparent difference for In at 115 amu, see Fig. 4). In the following, signals are labeled with a superscripts +,− or 0 to denote the charge state of the respective secondary particle. The peaks of the alkali metals $Na^+$ (23 amu) and $K^+$ (39 amu) are present in all six mass spectra. Their presence

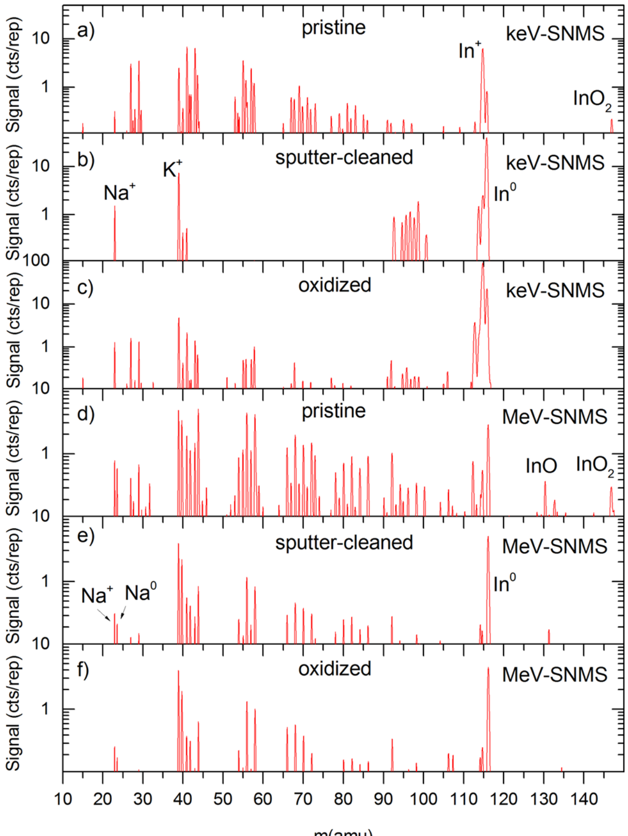


Fig. 1. (Color online) Secondary neutral mass spectra (SNMS) of indium with a molybdenum aperture under 5 keV $Ar^+$ [(a)–(c)] and 4.8 MeV/u $^{48}Ca^{10+}$ [(d)–(f)] bombardment for different surface compositions. The data was taken using a pulse particle current of 24 nA (SHI, flux density $3.8 \times 10^{11}$ ion/cm$^2$s) and 64 nA ($Ar^+$, flux density $5.7 \times 10^{12}$ ion/cm$^2$s), respectively. Signals of secondary neutrals are shifted 115 ns to higher masses (about 1 amu for In).

is not the result of a high abundance of these species at the surface but rather reflect the large SIMS ionization probability (close to unity) observed for these atoms under kilo-electron-volt ion bombardment. Surprisingly, $Na^0$ and $K^0$ signals are detected in the mega-electron-volt-SNMS spectra of Figs. 1(d)–1(f), which are not found under kilo-electron-volt bombardment. We observed this effect of neutral alkali emission for other metals as well and the reason is still unclear. The signals at masses 24–28 and 40–90 amu correspond mostly to hydrocarbons and are typical for samples exposed to ambient conditions during the sample preparation. The signals are completely removed in the kilo-electron-volt-SNMS spectrum for the sputter-cleaned surface but still present in the mega-electron-volt-SNMS. These signals probably originate from outer areas on the Mo aperture, which are being irradiated by the mega-electron-volt beam but not exposed to the smaller $Ar^+$ beam profile. Some of the peaks in the mass ranges 24–28 and 40–90 amu reappear for the oxidized surface [Fig. 1(c)] because of the adsorption of molecules from the residual gas. A $Mo^0$ signal with the characteristic Mo isotope distribution in the range 92–101 amu originating from the aperture is found for the sputter-cleaned surface in the kilo-electron-volt-SNMS spectrum [Fig. 1(c)]. This signal does not appear in the mega-electron-volt generated spectrum, reflecting the fact that good conducting metal samples are not efficiently sputtered under electronic stopping conditions. The $In^+$ peak at 115 amu can at this scale only be seen in the kilo-electron-volt spectra [Figs. 1(a) and 1(c)], but it is present in all measurements. The $In^0$ peak is shifted to an apparent mass of 116 amu and visible in all spectra. $InOH_2^{+,0}$ peaks are visible around 130 amu in Figs. 1(d) and 1(e) and $InO_2^+$ at 147 amu in Figs. 1(a) and 1(d). Not shown in this mass range are the $In_2X$ signals, which are only detected for the sputter-cleaned and oxidized surface. In the kilo-electron-volt spectra $In_2^{+,0}$ is visible as well as $In_2O^{+,0}$. A small (0.3 cts/rep) $In_2O^0$ peak is present in the mega-electron-volt-SNMS spectra for both the sputter-cleaned and the oxidized surface. The mega-electron-volt $In_2^{+,0}$ peaks are not discriminable from the background noise (<0.01 cts/rep).

Figure 2 shows the mass spectra measured for negative secondary ions under irradiation with 5 keV $Ar^+$ (a), (b) and 4.8 MeV/u $^{48}Ca^{10+}$ (c), (d) bombardment for the pristine (a), (c) and sputter-cleaned (b), (d) surface. At the lower mass range (<100 amu), $OH_2^-$ and $Cl^-$ (35 and 37 amu) as well as repeating groups of hydrocarbons are visible in all spectra. Although not directly noticeable at the logarithmic presentation, these signals are greatly reduced by the $Ar^+$ sputter cleaning. Most conspicuous at the higher mass scale are the isotopic distributions of $MoO_3^-$ (140–148 amu) and $MoO_4H^-$ (157–165 amu). The two smaller groups at mass range 165–190 amu exhibit the isotopic pattern of molybdenum but could not be explicitly identified. The large contribution to the mega-electron-volt signal, albeit originating from an area further away from the sensitive volume of the spectrometer, indicates a large sputter yield of the native molybdenum oxide. The only peak that can be clearly attributed to the indium is $InO^-$ at 136 amu.

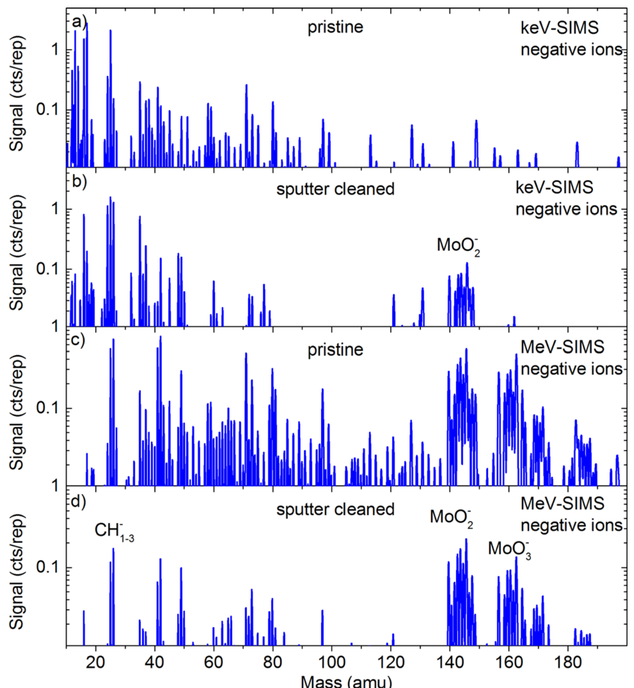


Fig. 2. (Color online) Negative secondary ion mass spectra measured at a polycrystalline indium surface covered with a molybdenum mask (aperture 2 mm) under 5 keV $Ar^+$ (a), (b) and 4.8 MeV/u $^{48}Ca^{10+}$ (c), (d) bombardment for different surface conditions. The data were taken using a pulse particle current of 24 nA ($Ca^{10+}$, flux density $3.8 \times 10^{11}$ ion/cm$^2$ s) and 64 nA ($Ar^+$, flux density $5.7 \times 10^{12}$ ion/cm$^2$ s), respectively.

A comparison of the $In^0$ peak areas in the mega-electron-volt- and kilo-electron-volt-SNMS spectra measured for the sputter-cleaned surface yields a factor of 8.3 lower signal for the mega-electron-volt bombardment. Considering the 15 times higher primary ion flux for 5 keV $Ar^+$ ions, one arrives at a 1.8-times higher $In^0$ signal per projectile impact for the mega-electron-volt ions. However, caution must be taken when directly relating the measured postionization signals to the sputter yield. Since the quantity measured here is the *number density* of sputtered particles within the sensitive volume of the spectrometer rather than their *flux*, a possible difference in the velocity distribution of the detected particles will alter the measured signal. More specifically, particles emitted with a higher average velocity would result in a lower particle density at the same sputter yield and vice versa. For kilo-electron-volt ion bombardment, the emission velocity spectrum has been measured[47,56] and can be well described by the linear cascade prediction.[57] Up till now, nothing is known about the emission velocity distribution of neutral atoms sputtered from an indium surface under mega-electron-volt ion bombardment conditions, so that the possible magnitude of this effect cannot be estimated. Another possible source of error is the thermal desorption of atoms induced by the heating of the sample during the mega-electron-volt irradiation, but this possibility can be excluded since no increase of the background gas signals was recorded.

In order to examine the possible role of nuclear sputtering, the SRIM software package[58] was used to calculate yield

values of 8.6 atoms/ion for 5 keV $Ar^+$ and 0.06 atoms/ion ($6 \times 10^{-3}$ keV/nm nuclear stopping power) for 230 MeV $^{48}Ca$ projectiles. Moreover, the velocities of the sputtered particles shown in these calculations are on average larger for the mega-electron-volt than for the kilo-electron-volt irradiation, which means that the relative contribution to the signal in our experiment would be even lower for the mega-electron-volt ions. The fact that the measured signal ratio is more than 2 orders of magnitude higher than the nuclear yield ratio calculated with SRIM therefore strongly indicates an electronic sputtering effect for 4.8 MeV/u $^{48}Ca^{10+}$ bombardment of indium. The electronic stopping power of the projectile ions is calculated as 6.4 keV/nm using the CASP software package[59] with the default parameters (UCA model, charge-state scan). In this context, it should be noted that we recently[60] obtained an even larger postionization signal for indium under 4.8 MeV/u $^{197}Au^{26+}$ irradiation with an electronic stopping power of 23 keV/nm (calculated with CASP).

## B. Depth profiles

Following the analysis of the pristine surface, the native oxide and the carbo-hydrate surface contaminations were removed while continually acquiring kilo-electron-volt and mega-electron-volt mass spectra using the interleaved sputter cleaning method.

The resulting sputter time (or $Ar^+$ ion fluence) dependence of a few relevant measured signals is displayed in Fig. 3. Panel (a) shows the profile observed for the oxide related indium signals $InOH_2{}^+$ and $In_2O^0$. In the kilo-electron-volt spectra, both signals exhibit a maximum at 250 s, followed by a slow decay. The initial rise is presumably due to a surface contamination with carbo-hydrates and other molecular species, which can be seen in Fig. 1(a). The corresponding $In^0$ signal displayed in panel (b) reaches 60% if its final value at a sputter time of 1000 s, corresponding to an $Ar^+$ ion fluence of about $6 \times 10^{15}$ ions/cm$^2$, suggesting that the transition between the native oxide layer and the underlying indium is occurring at this point. Using the sputter yield of 8.6 atoms/ion calculated with SRIM for pure indium, the corresponding sputter depth would be around 1.3 nm, indicating that the thickness of the native oxide layer on the as-introduced sample is of that order. It should be noted that this estimate might be subject to error, since the sputter yield of the native indium oxide may differ from the value for pure indium.

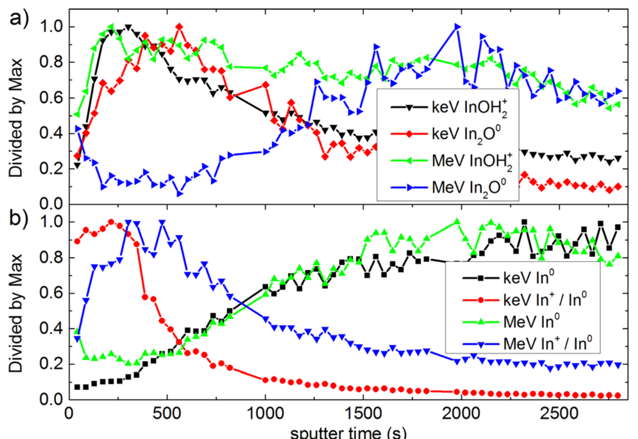


FIG. 3. (Color online) Normalized signals measured as a function of time during the interleaved sputter cleaning of the pristine surface. The superscripts 0 and + depict postionized neutrals and secondary ions, respectively. Primary ions used are 5 keV $Ar^+$ (keV) and 4.8 MeV/u $^{48}Ca^{10+}$ (MeV). The $Ar^+$ flux density was $5.7 \times 10^{12}$ ions/cm$^2$s. The total fluence of $^{48}Ca^{10+}$ for all data points was $1.6 \times 10^{14}$ ions/cm$^2$.

The $InOH^+$ and $In_2O^0$ signals generated by the 4.8 MeV/u $^{48}Ca^{10+}$ projectiles exhibit a significantly different trend than those generated by the kilo-electron-volt irradiation. Most significantly, the $In_2O^0$ signal shows a *minimum* during the exposure of the native oxide layer and *rises* when profiling into the pure indium solid. The $InOH_2{}^+$ signal, on the other hand, remains nearly constant after the initial rise. The remaining oxide signals observed at the end of the profile displayed in Fig. 3 might suggest that the surface area accessible by the mega-electron-volt beam is not completely sputter-cleaned by the $Ar^+$ ion bombardment. However, the strong dependence on the $Ar^+$ ion fluence observed at the beginning of the depth profile limits the possible significance of this error, and the rise observed for the $In_2O^0$ signal certainly cannot be explained this way. A second possible source for the oxygen is the readsorption from the residual gas during the relatively long (5 ms) UNILAC pulse where the continuous $Ar^+$ bombardment is switched off.

The trend of the $In^+$ to $In^0$ ratio displayed in Fig. 3(b) shows interesting differences between kilo-electron-volt and mega-electron-volt primary ions. The kilo-electron-volt profile starts with a plateau in the native oxide layer and shows a significantly stronger decay compared to the kilo-electron-volt-generated oxide molecule signals. This demonstrates that the surface contamination as well as the oxide greatly increases the ionization probability of the indium atoms, which is a well-known effect kilo-electron-volt-SIMS experiments. The ion fraction observed under mega-electron-volt irradiation, on the other hand, does not appear to be enhanced by the uppermost surface contamination, but reflects a clear increase of the ionization probability within the native oxide layer. While the ionization probability observed under kilo-electron-volt impact decays to practically zero in the pure indium solid, that observed under mega-electron-volt irradiation appears to level off at a significantly larger value.

## C. Surface oxidation

Following the sputter cleaning process, the clean indium surface was reoxidized by introducing an $O_2$ partial pressure of $5 \times 10^7$ mbar into the analysis chamber. An extended view of the mass spectra measured for secondary indium atoms and ions at the sputter-cleaned and reoxidized surface is shown in Fig. 4. The mass scale was calibrated for the secondary ions, and the postionized neutral peaks are shifted upward by about 1 apparent mass unit due to the applied 115 ns laser delay. Note that the spectra recorded in SNMS mode contain the SIMS spectrum as well, albeit with less

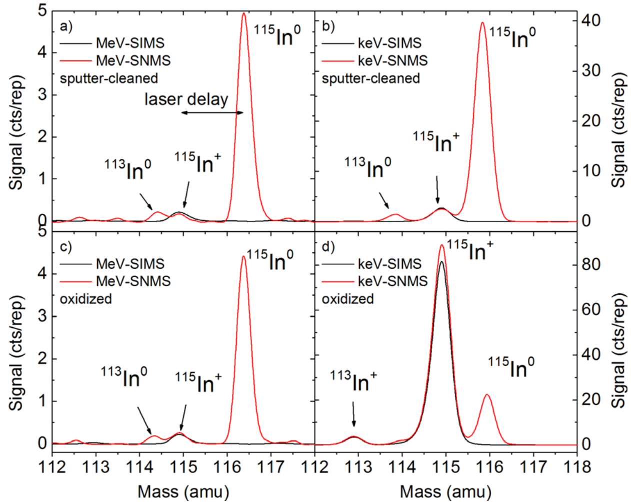


FIG. 4. (Color online) Mass spectra of secondary indium ions ($In^+$) and postionized neutral atoms ($In^0$) measured for a sputter-cleaned [(a), (b)] and oxidized [(c), (d)] indium surface under 5 keV $Ar^+$ [(b), (d)] and 4.8 MeV/u $^{48}Ca^{10+}$ [(a), (c)] bombardment. The data were taken using a pulse particle current of 24 nA (SHI, flux density $3.8 \times 10^{11}$ ion/cm$^2$s) and 64 nA ($Ar^+$, flux density $5.7 \times 10^{12}$ ion/cm$^2$s), respectively. Signals for secondary ions and neutrals are separated by a 115 ns laser delay, and the mass scale was calibrated for secondary ions.

counting statistics due to the lower number of repetitions used for SNMS acquisition. Note also the similar peak shapes recorded for secondary ions and postionized neutrals, which provide strong indication that the postionization laser homogenously illuminates the entire sensitive volume of the mass spectrometer.

Comparing the $^{115}In^+$ and $^{115}In^0$ signals measured for the sputter-cleaned surface [panels (a) and (b) in Fig. 4], one finds an ion/neutral ratio of about 10% under kilo-electron-volt ion bombardment, which probably overestimates the true ionization probability due to incomplete saturation of the postionization efficiency. This overestimation, however, is not important for the conclusions of the present work, since here we are interested in relative variations of the ionization probability as a function of the surface chemistry, which does not influence the postionization efficiency. Looking at panels (c) and (d) of Fig. 4, one immediately sees that kilo-electron-volt- and mega-electron-volt-induced spectra react on surface oxidation in a different way. In the kilo-electron-volt spectrum, the secondary ion peak strongly grows and becomes the major detected signal, while at the same time the $In^0$ peak is decreased. Both findings are expected since the ionization probability is known to be enhanced by the presence of surface oxygen, while the signal of sputtered neutral indium atoms represents the indium surface concentration, which is diminished with increasing oxygen coverage. The surprising observation in Fig. 4 is that the mega-electron-volt-generated signals do not show a similar behavior. Comparing the spectra displayed in panels (a) and (c) of the figure, one finds that the signals of both the secondary ions and the postionized neutral atoms appear virtually unchanged by the oxygen exposure.

Figure 5 displays the development of the In and $In_2O$ signals obtained under 5 keV $Ar^+$ and 4.8 MeV/u $^{48}Ca^{10+}$

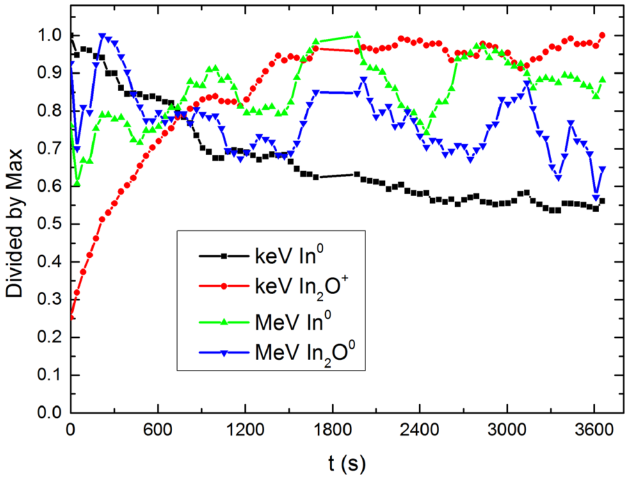


FIG. 5. (Color online) Normalized trend for In and $In_2O$ signals for 5 keV $Ar^+$ (keV) and 4.8 MeV/u $^{48}Ca^{10+}$ (MeV) primary ions during the oxidation of the surface with $5 \times 10^7$ mbar partial pressure of $O_2$.

irradiation as a function of oxygen exposure time. The kilo-electron-volt-induced $In_2O^+$ signal was chosen for display here because of the low level and poor statistics of the $In_2O^0$ signal measured under these irradiation conditions. The temporal evolution of this signal reflects the expected deposition of oxygen on the surface, albeit possibly overestimating the actual variation of the oxygen concentration since not only the partial sputter yield but also the ionization probability of the $In_2O$ molecule may also greatly increase with increasing oxygen surface concentration. As noted earlier, the kilo-electron-volt-induced $In^0$ signal shows the expected decrease with increasing oxygen coverage. The signal converges to about 50% of that measured at the sputter-cleaned surface, thus roughly indicating an InO stoichiometry of the fully oxidized surface. The corresponding signals measured under mega-electron-volt ion irradiation show no distinct trend during the oxidation of the surface. The observable signal variation can mostly be attributed to instabilities in the UNILAC ion current (leading to a parallel variation of all signals) and poor statistics due to the overall low signal level. Unfortunately, it was not possible to increase the signal level by boosting the mega-electron-volt primary ion flux in order to prevent any fluence effects or heating of the sample during the measurement.

The variation of the ion to neutral signal ratio for indium atoms sputtered under 5 keV $Ar^+$ and 4.8 MeV/u $^{48}Ca^{10+}$ bombardment is displayed in Fig. 6 as a function of oxygen exposure time. The data points taken during the oxidation run have been complemented with a measurement taken after an extended period of sputter cleaning the surface after completion of the oxidation experiment. The $Ar^+$ ion fluence accumulated during the 11.5 h cleaning period was $2.3 \times 10^{17}$ ions/cm$^2$ with an estimated removal of 54 nm of the indium sample. Despite being acquired later, the respective data points have been added on the left-hand side of the diagram since they represent a thoroughly sputter-cleaned and thus nearly oxygen free surface. The remaining residual oxygen surface concentration is determined by a dynamic

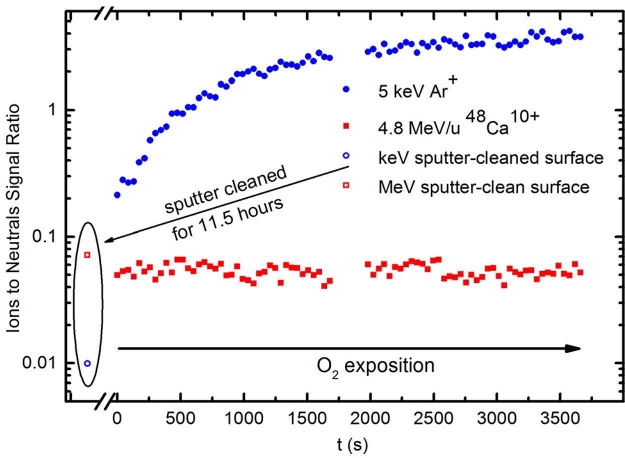


FIG. 6. (Color online) $^{115}In^+$ to $^{115}In^0$ signal ratio for 5 keV $Ar^+$ and 4.8 MeV/u $^{48}Ca^{10+}$ primary ions measured as a function of time during the exposition of the surface to $5 \times 10^{-7}$ mbar partial pressure of $O_2$. The total ion fluence accumulated during the 3600 s of oxidation was $2.1 \times 10^{14}$ and $2.5 \times 10^{12}$ ions/cm$^2$ for 4.8 MeV/u $^{48}Ca^{10+}$ and the 5 keV $Ar^+$ ions, respectively. The two data points depicted on the left-hand side are not connected to the time scale but were obtained by sputter cleaning the surface again for 11.5 h ($2.3 \times 10^{17}$ ions/cm$^2$ $Ar^+$) after the $O_2$ exposition.

equilibrium between readsorption and sputter removal of oxygen. Using an ion flux density of $5 \times 10^{12}$ ions/cm$^2$s, a sputter yield of ten atoms per ion and a residual gas pressure $\sim 10^{-9}$ mbar, one obtains an equilibrium oxygen surface concentration of about 0.5 at. %. It is seen that the ionization probability measured under these conditions is still by a factor 20 lower than that measured at the beginning of the oxidation experiment (which was started with a nominally sputter-cleaned surface).

Upon oxygen exposure, the secondary indium atoms sputtered under 5 keV $Ar^+$ bombardment exhibit the well-known oxygen matrix effect with their ionization probability being increased by more than 2 orders of magnitude between the cleaned and oxidized surface. In marked contrast, no such trend is observable during the entire oxidation period for the $In^+$ ions generated under 4.8 MeV/u $^{48}Ca^{10+}$ bombardment (Fig. 6). This finding points to a fundamental difference between the emission processes for the particles sputtered under kilo-electron-volt and mega-electron-volt irradiation, respectively. In the nuclear sputtering regime explored here, particles are mainly removed from the uppermost layer by recoils of a linear collision cascade. For an oxygen-covered surface, the indium atoms sputtered under these conditions are removed from an InO-matrix, where almost every emitted atom has at least one oxygen atom as nearest neighbor. The breaking of this bond results in a strong influence on the charge state of the emitted atom. For the electronic-sputtering, on the other hand, energy must first be transferred from the electrons to the lattice via electron-phonon coupling. As a result, particles are emitted from a small heated volume and may exhibit a more collective transition into the vacuum comparable to a phase explosion. The emission of particles from an excited cylindrical volume of a swift heavy ion track has been investigated using molecular dynamics (MD) simulations by Bringa *et al.*[61] and recently by our group as well.[62] The results of the simulations show a significantly larger contribution of atoms originating from subsurface layers as compared to the kilo-electron-volt impact induced sputtering process. While the oxygen adsorbed under UHV conditions is located exclusively at the surface, where it becomes ejected in the beginning of the sputtering process where the surface is being disrupted, a particle originating from a deeper layer is ejected at later times and cannot be affected by any surface contaminant. A similar observation is made in kilo-electron-volt sputtering, when the atomic projectile is replaced by a cluster. Also in this case, the sputtering process changes from linear collision cascade to a phase explosion, and the ionization probability of sputtered atoms is found to be less affected by surface contamination.[63] This emission from deeper layers is in agreement with the increase of the ionization probability found for the thicker native oxide (Fig. 3), as well as the larger $In^0$ signal for the pristine surface in contrast to the kilo-electron-volt spectrum. In a different measurement[60] performed under 4.8 MeV/u $^{48}Ca^{10+}$ irradiation, we found indications for a more forward directed emission of indium atoms as compared to 5 keV $Ar^+$, which would also point toward a more collective ejection of particles.

Another interesting result is the four to sevenfold increased ionization probability for the thoroughly sputter-cleaned surface (Fig. 6). Given the strong dependence of the kilo-electron-volt-SIMS signal on oxygen residues on the surface, this factor represents a lower limit and may still increase if a larger ion current is used for the interleaved sputter cleaning. The increased ionization probability under mega-electron-volt bombardment could be interpreted as a remnant of the initial electronic excitation, still present at the time when the particles are emitted. The initial electronic excitation usually dissipates in metals even before any significant energy transfer to the lattice can occur. However, since our data clearly shows evidence for electronic sputtering for indium, it can be concluded that this dissipation is somehow reduced, possibly due to the fast melting of the area around the ion track.

## IV. SUMMARY AND CONCLUSIONS

The experiments on sputtering of indium under SHI (4.8 MeV/u $^{48}Ca^{10+}$) irradiation presented here show indications of a fundamentally different particle ejection mechanism as compared to the collisional sputtering process observed under 5 keV $Ar^+$ bombardment. The measured signals of postionized secondary neutral indium atoms are comparable for both projectiles, while calculations performed with SRIM show a 2 orders of magnitude lower nuclear sputtering yield for the 4.8 MeV/u $^{48}Ca^{10+}$ ions. Therefore, the detected sputter yield must be connected to the electronic stopping of those projectiles with a stopping power of 6.4 keV/nm (calculated with CASP). For a thoroughly sputter-cleaned surface, a significant increase in the ionization probability of sputtered indium atoms is measured under SHI bombardment, which could be connected to the initial electronic excitation of the sample. The presence of a native oxide layer on the pristine indium

surface acts to increase the ionization probability measured under SHI irradiation, while a monolayer oxygen coverage deposited on a previously sputter-cleaned surface has no detectable influence on the ionization probability. Particularly the latter finding is in strong contrast to the kilo-electron-volt ion bombardment experiments, which exhibit an increase in the ionization probability by more than 2 orders of magnitude due to the known oxygen matrix effect. A possible explanation is given by the depth of origin distribution of the emitted atoms. Under 5 keV $Ar^+$ irradiation, more than 90% of the sputtered material originates from the uppermost layer and is therefore strongly influenced by the presence of oxygen at the surface. The source of particles emitted under electronic sputtering conditions on the other hand, is an excited cylindrical track. MD simulations of the resulting particle emission process reveal a phase explosion, leading to a larger contribution of emitted particles originating from deeper layers. The particles are emitted at later times and never "see" the initial surface contamination, which has been removed in the early stages of the sputtering process. They are, however, influenced by oxygen atoms buried in a thicker native oxide layer.

## ACKNOWLEDGMENTS

The authors are greatly indebted to W. Saure and A. Siegmund for technical assistance during the setup of the experiment. The authors also acknowledge financial support from the German Ministry of Science (BMBF) in the framework of the Verbundprojekt Nos. 05K13PG1 and 05K16PG1 "Ion Induced Materials Characterization and Modification."

[1]R. Behrisch *et al.*, *Sputtering by Particle Bombardment Vols. I–IV*, edited by R. Behrisch, K. Wittmaack, and W. Eckstein (Springer, Berlin, 1981;1983;1991;2007).
[2]H. M. Urbassek and W. O. Hofer, in *Fundamental Processes in Sputtering of Atoms and Molecules (SPUT92)*, 43rd ed., edited by P. Sigmund (Det Kongelige Danske Videnskabernes Selskab, Copenhagen, 1993), p. 97.
[3]*Ion Beam Science: Solved and Unsolved Problems*, Matematisk-Fysiske Meddelelser 52, edited by P. Sigmund (Det Kongelige Danske Videnskabernes Selskab, Copenhagen, 2006).
[4]W. Assmann, M. Toulemonde, and C. Trautmann, in *Sputtering by Particle Bombardment*, edited by R. Behrisch and W. Eckstein (Springer, Berlin, 2007), Vol. 110, p. 401.
[5]Z. E. Switkowski, F. M. Mann, D. W. Kneff, R. W. Ollerhead, and T. A. Tombrello, Radiat. Eff. Defect Solids **29**, 65 (1976).
[6]Y. X. Qiu, J. E. Griffith, and T. A. Tombrello, Nucl. Instrum. Methods, B **1**, 118 (1984).
[7]M. Toulemonde, W. Assmann, C. Trautmann, and F. Gruner, Phys. Rev. Lett. **88**, 057602 (2002).
[8]H. D. Mieskes, W. Assmann, F. Gruner, H. Kucal, Z. G. Wang, and M. Toulemonde, Phys. Rev. B **67**, 155414 (2003).
[9]M. Toulemonde, W. Assmann, C. Trautmann, F. Gruner, H. D. Mieskes, H. Kucal, and Z. G. Wang, Nucl. Instrum. Methods, B **212**, 346 (2003).
[10]S. A. Khan, A. Tripathi, M. Toulemonde, C. Trautmann, and W. Assmann, Nucl. Instrum. Methods, B **314**, 34 (2013).
[11]A. Meftah, W. Assmann, N. Khalfaoui, J. P. Stoquert, F. Studer, M. Toulemonde, C. Trautmann, and K. O. Voss, Nucl. Instrum. Methods, B **269**, 955 (2011).
[12]M. Toulemonde, W. Assmann, and C. Trautmann, Nucl. Instrum. Methods, B **379**, 2 (2016).
[13]M. Toulemonde, W. Assmann, D. Muller, and C. Trautmann, Nucl. Instrum. Methods, B **406**, 501 (2017).
[14]M. R. Weller, K. M. Hubbard, R. A. Weller, D. L. Weathers, and T. A. Tombrello, Nucl. Instrum. Methods, B **42**, 19 (1989).
[15]W. Assmann *et al.*, Nucl. Instrum. Methods, B **392**, 94 (2017).
[16]A. L'Hoir *et al.*, Nucl. Instrum. Methods, B **267**, 876 (2009).
[17]H. Hijazi *et al.*, Nucl. Instrum. Methods, B **269**, 1003 (2011).
[18]H. Hijazi, L. S. Farenzena, H. Rothard, P. Boduch, P. L. Grande, and E. F. da Silveira, Eur. Phys. J. D **63**, 391 (2011).
[19]H. Hijazi *et al.*, Eur. Phys. J. D **66**, 68 (2012).
[20]H. Hijazi, T. Langlinay, H. Rothard, P. Boduch, F. Ropars, A. Cassimi, L. S. Farenzena, and E. F. da Silveira, Eur. Phys. J. D **68**, 185 (2014).
[21]R. Martinez, T. Langlinay, P. Boduch, A. Cassimi, H. Hijazi, F. Ropars, P. Salou, E. F. da Silveira, and H. Rothard, Mater. Res. Express **2**, 076403 (2015).
[22]C. C. de Castro, I. S. Bitensky, and E. F. da Silveira, Nucl. Instrum. Methods, B **132**, 561 (1997).
[23]J. A. M. Pereira, E. F. Da Silveira, and K. Wien, Radiat. Eff. Defect Solids **142**, 247 (1997).
[24]J. A. M. Pereira and E. F. da Silveira, Nucl. Instrum. Methods, B **155**, 206 (1999).
[25]J. A. M. Pereira, I. S. Bitensky, and E. F. da Silveira, Nucl. Instrum. Methods, B **135**, 244 (1998).
[26]C. C. de Castro, I. S. Bitensky, E. F. da Silveira, M. Most, and K. Wien, Int. J. Mass Spectrom. **173**, 1 (1998).
[27]J. A. M. Pereira, I. S. Bitensky, and E. F. da Silveira, Int. J. Mass Spectrom. **174**, 179 (1998).
[28]J. A. M. Pereira and E. F. da Silveira, Nucl. Instrum. Methods, B **136**, 779 (1998).
[29]J. A. M. Pereira and E. F. da Silveira, Phys. Rev. Lett. **84**, 5904 (2000).
[30]F. A. Fernandez-Lima, O. P. VilelaNeto, A. S. Pimentel, C. R. Ponciano, M. A. C. Pacheco, M. A. C. Nascimento, and E. F d. Silveira, J. Phys. Chem. A **113**, 1813 (2009).
[31]F. Alberto Fernandez-Lima, O. P. Vilela Neto, A. Silva Pimentel, M. A. C. Pacheco, C. R. Ponciano, M. A. C. Nascimento, and E. F. da Silveira, J. Phys. Chem. A **113**, 15031 (2009).
[32]H. Oechsner and E. Stumpe, Appl. Phys. **14**, 43 (1977).
[33]D. Lipinsky, R. Jede, J. Tümpner, O. Ganschow, and A. Benninghoven, J. Vac. Sci. Technol. **3**, 2035 (1985).
[34]A. Wucher, in *TOF-SIMS: Materials Analysis by Mass Spectrometry*, 2nd ed., edited by J. C. Vickerman and D. Briggs (IM Publications/SurfaceSpectra, Chichester/Manchester, 2013), p. 217.
[35]J. B. Pallix, U. Schuhle, C. H. Becker, and D. L. Huestis, Anal. Chem. **61**, 805 (1989).
[36]N. P. Lockyer and J. C. Vickerman, Laser Chem. **17**, 139 (1997).
[37]M. Wahl and A. Wucher, Nucl. Instrum. Methods, B **94**, 36 (1994).
[38]L. K. Takahashi, J. Zhou, K. R. Wilson, S. R. Leone, and M. Ahmed, J. Phys. Chem. A **113**, 4035 (2009).
[39]I. V. Veryovkin, W. F. Calaway, J. F. Moore, M. J. Pellin, J. W. Lewellen, Y. L. Li, S. V. Milton, B. V. King, and M. Petravic, Appl. Surf. Sci. **231**, 962 (2004).
[40]L. Hanley, P. D. Edirisinghe, W. F. Calaway, I. V. Veryovkin, M. J. Pellin, and J. F. Moore, Appl. Surf. Sci. **252**, 6723 (2006).
[41]A. Wucher, W. Berthold, and H. Oechsner, in *Secondary Ion Mass Spectrometry (SIMS IX)* (Wiley, Yokohama, 1993), p. 100.
[42]A. Wucher, R. Heinrich, R. M. Braun, K. F. Willey, and N. Winograd, Rapid Commun. Mass Spectrom. **12**, 1241 (1998).
[43]R. Heinrich and A. Wucher, Nucl. Instrum. Methods, B **140**, 27 (1998).
[44]R. Heinrich, C. Staudt, M. Wahl, and A. Wucher, in *Secondary Ion Mass Spectrometry (SIMS XII)* (Elsevier Science, Amsterdam, 1999), p. 111.
[45]A. Wucher, R. Heinrich, and C. Staudt, in *Secondary Ion Mass Spectrometry (SIMS XII)* (Elsevier Science, Amsterdam, 1999), p. 143.
[46]C. Staudt, R. Heinrich, and A. Wucher, Nucl. Instrum. Methods, B **164–165**, 677 (2000).
[47]C. Staudt and A. Wucher, Phys. Rev. B **66**, 075419 (2002).
[48]S. Meyer, C. Staudt, and A. Wucher, Appl. Surf. Sci. **203–204**, 48 (2003).
[49]A. V. Samartsev and A. Wucher, Appl. Surf. Sci. **252**, 6474 (2006).
[50]P. Mazarov, A. V. Samartsev, and A. Wucher, Appl. Surf. Sci. **252**, 6452 (2006).
[51]J. München, D. Lipinsky, and H. F. Arlinghaus, Surf. Interface Anal. **45**, 117 (2013).
[52]A. Benninghoven, Surf. Sci. **53**, 596 (1975).
[53]A. Wucher and H. Oechsner, Surf. Sci. **199**, 567 (1988).
[54]F. Meinerzhagen, L. Breuer, H. Bukowska, M. Bender, D. Severin, M. Herder, H. Lebius, M. Schleberger, and A. Wucher, Rev. Sci. Instrum. **87**, 013903 (2016).

[55]A. Wucher, M. Wahl, and H. Oechsner, Nucl. Instrum. Methods, B **82**, 337 (1993).
[56]Z. Ma, W. F. Calaway, M. J. Pellin, and E. I. von Nagy-Felsobuki, Nucl. Instrum. Methods, B **94**, 197 (1994).
[57]M. W. Thompson, Philos. Mag. **18**, 377 (1968).
[58]J. F. Ziegler, M. D. Ziegler, and J. P. Biersack, Nucl. Instrum. Methods, B **268**, 1818 (2010).
[59]G. Schiwietz and P. L. Grande, Phys. Rev. A **84**, 052703 (2011).
[60]L. Breuer, P. Ernst, M. Herder, F. Meinerzhagen, M. Bender, D. Severin, and A. Wucher, "Mass spectrometric investigation of material sputtered under swift heavy ion bombardment," Nucl. Instrum. Methods, B (published online).
[61]E. M. Bringa, R. E. Johnson, and M. Jakas, Phys. Rev. B **60**, 15107 (1999).
[62]P. Kucharczyk, A. Füngerlings, A. Wucher, and B. Weidtmann, "Computer simulation of sputtering induced by swift heavy ions," Nucl. Instrum. Methods, B (submitted).
[63]A. V. Samartsev, C. Heuser, and A. Wucher, Surf. Interface Anal. **45**, 87 (2012).